

Experimental static and dynamic tests on a large-scale free-form Voronoi grid shell mock-up in comparison with finite-element method results

Maurizio Froli¹ · Francesco Laccone¹ 

Received: 9 February 2016 / Accepted: 15 July 2017 / Published online: 24 July 2017
© The Author(s) 2017. This article is an open access publication

Abstract Grid shells supporting transparent or opaque panels are largely used to cover long-spanned spaces because of their lightness, the easy setup, and economy. This paper presents the results of experimental static and dynamic investigations carried out on a large-scale free-form grid shell mock-up, whose geometry descended from an innovative Voronoi polygonal pattern. Accompanying finite-element method (FEM) simulations followed. To these purposes, a four-step procedure was adopted: (1) a perfect FEM model was analyzed; (2) using the modal shapes scaled by measuring the mock-up, a deformed unloaded geometry was built, which took into account the defects caused by the assembly phase; (3) experimental static tests were executed by affixing weights to the mock-up, and a simplified representative FEM model was calibrated, choosing the nodes stiffness and the material properties as parameters; and (4) modal identification was performed through operational modal analysis and impulsive tests, and then, a simplified FEM dynamical model was calibrated. Due to the high deformability of the mock-up, only a symmetric load case configuration was adopted.

Keywords Free form · Grid shell · Voronoi · Polygonal pattern · Experimental static test · Operational modal analysis · Impulsive test

Introduction

Contextualization of the work

As spatial lightweight structures, free-form constructions played a prominent role in recent years thanks to more reliable computational techniques, increased knowledge of building materials, and new architectural expressivity. Long-spanned free-form roofs and building skins are realized as grid shells connecting a set of discrete (opaque or transparent) panels to a supporting grid structure. Before the structural aspects, the engineering process of the geometrical and constructional definition of the faceted architectural shape is related to the feasibility and the modalities of the base-surface subdivision (Adriaenssens et al. Adriaenssens et al. 2012, 2014; Baldassini et al. 2010; Pottmann 2013; Pottmann et al. 2007; Sassone and Pugnale 2010).

Grid shells are afflicted by some static problems as deformability, buckling, and imperfection sensitivity (Schlaich and Schober 1996, 1997) and by constructional problems such as nodes assembly, feasibility of the panels geometry and curvature, connectivity of the elements, etc. because of their three-dimensional spatial complexity. Therefore, a large displacement analysis typically applies to a grid shell due to the intrinsic deformability caused by its lightness. As they carry loads mainly by compressive forces, buckling failures (local, global, snap-through, or even worse combinations of previous) should be avoided. Stability analysis is carried out considering both second-order effects and imperfections, and a strong abatement of the buckling multiplier with respect to the ideally perfect structure is usually detected (Bacco and Borri 1993; Bulenda and Knippers 2001; Cai et al. 2013; Dini et al. 2013; Gioncu 1995).

✉ Francesco Laccone
francesco.laccone@destec.unipi.it

¹ Department of Energy, Systems, Territory and Construction Engineering, University of Pisa, Largo Lucio Lazzarino n. 1, 56126 Pisa, Italy

Typically, in the structural analysis of a grid shell, the influence of the panel is omitted as long as the simulation of the overall behavior is concerned, neglecting the interaction with the supporting structure in terms of strength or stiffness. The panel is considered essentially as a dead load weighing on the structural nodes.

Our contribution

Nowadays, the use of polygonal patterns in grid shells (Jiang et al. 2014, 2015; Pottman 2009) inspired by organic shapes is growing. Their structural lightness, their interesting geometrical properties, and aesthetic appeal favor them in comparison with their triangular and quad competitors. Optimization procedures are often iterative and provide for shape alterations to increase structural shell features. On the contrary, Pietroni et al. (2015) introduced an algorithm to mesh assigned free-form continuous shell surfaces by means of Voronoi polygonal patterns, whose procedure is affected by the membrane stresses acting on the initial shell. Practically, the tessellation, the density, and the anisotropy of the cells can be altered with respect to the statics of the initial continuous surface, driven by some control parameters. As stated, Voronoi static-aware grid shells manifested good static performances, better than the state-of-the-art competitors (Tonelli 2015). Furthermore, since the propensity to buckle of grid shells, Tonelli et al. (2016a) devoted a specific study to the stability and imperfection sensitivity analyses of hex-dominant free-form grid shells generated with the Statics Aware Voronoi algorithm. As a result, under some specific hypotheses (uniform loading, rigid joints, and pinned boundary), the outcomes confirmed the static efficiency. In particular, the bigger the irregularity of the initial continuous shell, the better the static performances of the Voronoi grid shell.

Even though such algorithm was tested from a computational viewpoint, up to now, feasibility studies and experimentations are missing. Moreover, a knowledge gap was noticed in the assessment of the node stiffness that can influence the theoretical stresses and displacement fields. The previous modelling assumptions concerning the connections are barely achievable. The stiffness of the joints plays a significant role; and to such an extent if as an extreme case, we remove the rigid joints condition, and the polygonal mesh becomes a mechanism. We referred to experimental observations.

Due to the novelty of this type of structural geometry and the dependency of the structural behavior on the initial shell and on the remeshing pattern, we decided to focus on a representative case study: a modern free-form vault (Fig. 1), whose geometry is based on the need to have a sufficiently complex model, but provided with multiple symmetry planes. The structure and its internal Voronoi

tessellation present four axes of symmetry: two parallel to reference X and Y global axes and two rotated by 45° (Fig. 2). Moreover, its plan is inscribable into a square figure, whose corner vertices are in a raised position, and whose mid-side points are the four ground anchor points. The global shape of the vault is an inverted catenary surface and the internal Voronoi net is predominantly axial stressed. Its large-scale replica was fabricated at the Structural Laboratory of the University of Pisa and its size is 2.40 m side. The mock-up is composed by 697 wooden beams, 462 laser-cutted PET (Polyethylene terephthalate) thin panels, and 465 FDM (Fused Deposition Modelling) printed joints (Fig. 3). The design and the assembly followed the automated approach, as shown in Tonelli et al. (2016b). The nomenclature used in the following refers to Fig. 2.

Because of the mechanical and geometric complexity, as first goal, the research focused on the theoretical behavior of the case study vault to identify the displacement field, the main load paths, and the modal properties under the assumption of rigid joints, fixed supports, and characteristic material properties. This part of the study was led on an FEM model, in the following named 'perfect', whose metric is that one generated by the Voronoi algorithm. Such model, as well as the following, adopted the same mock-up size.

In spite of the first modelling assumption of perfect geometry, the assemblage of the mock-up produced small defects related to materials, dimensional tolerances, difficulties of the assembling operations, particular shape of the shell structure, and local non-linearities (Pietroni et al. 2015; Tonelli et al. 2016a). We conveniently decided to consider the physical replica state introducing an inelastic deformation field in a further numerical model. The field was obtained from calibration of the modal eigenforms derived from the perfect geometry FEM model on the survey made on the prototype. Such model constituted the base geometry for numerical models analyzed in the following phase.

The second goal of this study was to execute non-destructive tests and consequently simulate the observed mock-up behavior with simplified FEM models. We performed two sets of experimental campaigns. The first set intended to investigate the statics of the mock-up, submitted to symmetrical loading patterns. The descending representative FEM static model did not consider the presence of the PET panels. Moreover, to approach the experimental behavior, we varied the beams rotational end-release stiffness and reduced the characteristic material properties, simulating the non-rigid connectivity, the local non-linearities, and structural imperfections.

The second experimental set aimed at the dynamic identification of the prototype. We acquired the modal

properties to understand the dynamic behavior of such structure, so to obtain information about the distribution of mass, stiffness, and damping. In the accompanying representative FEM dynamic model, we considered the structural response of both the supporting grid structure and the panels.

Analysis method and tests

The work can be divided into four main phases.

1. Theoretical behavior of the static-aware Voronoi case study. A numerical model was based on the geometry directly descended from the processes of static-aware form genesis. Since the FEM model and the mock-up have the same scale, the numerical results correspond to the theoretical behavior of the prototype. We refer to this phase as 'perfect geometry modelling'.
2. Study of the mock-up state. The aim is to define a displacement vector field to simulate the deformed unloaded mock-up state. Such displacement vector field was introduced as an inelastic deformation in the following numerical models.
3. Realization of static experimental tests. We processed, collected, and analyzed test-observed data, and finally, we generated a simplified FEM static representation in reverse fitting procedure.
4. Realization of dynamic experimental tests. The specific aims are the dynamic identification and the calibration of an FEM dynamic model.

The present study relied on three base assumptions regarding non-linearity, size of the models, and symmetry. In the non-linear static analyses, only geometrical non-linearity was included. Because the field of proportionality between stress and consequent displacement was indeed not exceeded, material non-linearity was omitted.

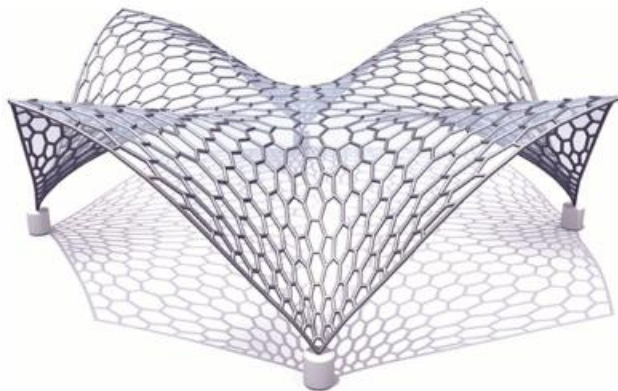


Fig. 1 Case study of a static-aware Voronoi free-form grid shell vault (Pietroni et al. 2015)

Moreover, other non-linearities were omitted such as contact and friction at the nodes. Concerning the size, FEM models conveniently represent the real size of the prototype (2.40 m side), avoiding to extend the structural test results to a larger scale model and to introduce further uncertainty. Among multiple loading configurations, we considered only symmetrical load cases in accordance with the symmetry of the vault. Other possible and probably more dangerous loading configurations may be asymmetrical loads. However, the Voronoi Static-Aware algorithm is still limited to the optimization of only symmetrically loaded surfaces (i.e., under dead loads, Pietroni et al. 2015; Tonelli et al. 2016a; Tonelli 2015); consequently, the high deformability of the mock-up excluded to extend the study to other loading scenarios.

Perfect geometry modelling (phase 1)

The first numerical model, named GS_0 , intended to test the static-aware Voronoi algorithm on the case study surface and to simulate the theoretical behavior of the mock-up. The properties were set as follows. The circular wooden beam sections were 8 mm diameter with Young's modulus $E = 11,000 \text{ N/mm}^2$. The PET panels were 1 mm thick with $E_p = 3700 \text{ N/mm}^2$. The prototype was installed on an OSB base panel by means of four stiff FDM special nodes. The latter are fixed through four screws on it. All the internal nodes were three-way connections. The beams were fitted into a 10 mm deep nodal plastic casing. Neither bolted nor glued connection was practiced. The mutual mechanical interaction between nodes and beams was by contact in case of beam compression, while only the friction limited the sliding in case of traction. Shear and bending were fully transmitted from beams to nodes. At this stage, in the FEM model, all the nodes of GS_0 were estimated as rigid, in a simplified approach. External constraints were supposed as all fixed joints, thanks to the stiffness of the OSB base panel. Material properties are defined as their characteristic values.

The PET panel is point supported at its vertices, which resulted clamped between the printed plastic node and a metallic washer screwed on the node itself. So that, given a non-linear constraint condition, the panel can detach and slide in case of tension stress. No direct contact is between the panels and the beams. After the attempt to include the panels into the model, we considered only their dead load: gravitational masses weighing 50 g were loaded at each node as simulating the printed joint and the panel influence. Since the aim was to provide a global simplified representation of the mock-up, requiring an in-depth modelling the complexity of the panels, joinery system would not have been compatible with a less refined global modelling



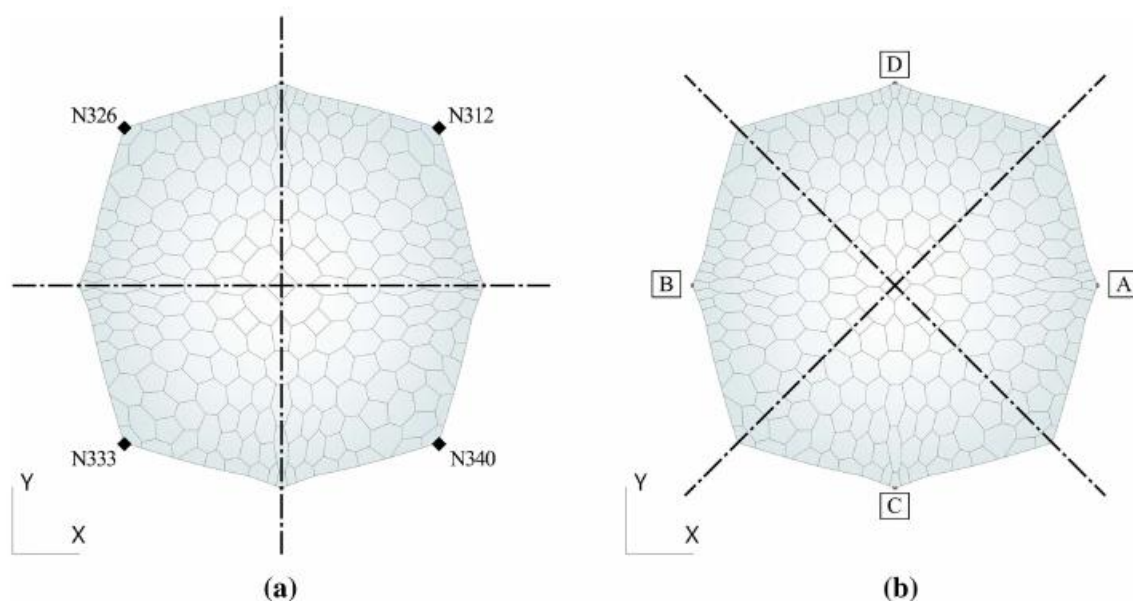


Fig. 2 Top view of the mock-up with evidenced symmetry axes: **a** nomenclature of the end corners and **b** base connection (A–D)

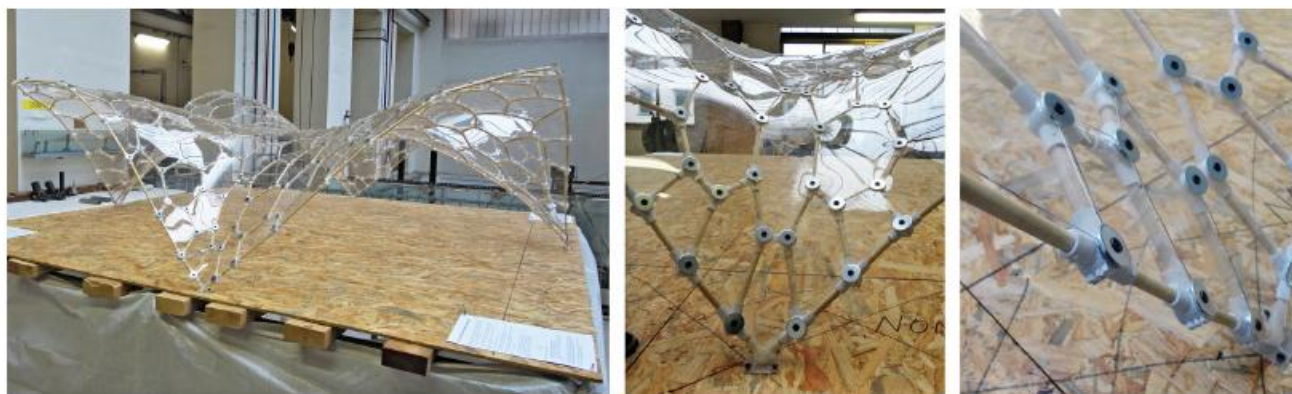


Fig. 3 Mock-up of static-aware Voronoi free-form grid shell vault at the Structural Laboratory of the University of Pisa

scale. Finally, the model consisted of 465 nodes and 697 beam elements.

Linear static analysis performed on the perfect geometry under own weight showed an expected prevailing compression regime: higher axial stresses were in areas close to the base constraints (Fig. 4a), where the Voronoi pattern has more stretched cells, in compliance with the property of stress field anisotropy (Pietroni et al. 2015). The main load paths are two compressed arches connecting the pair of opposite supports. The structure deformed in the gravity direction, except for the tops of the vault (corner vertices) that were dragged upward by the displacement of its center to the bottom (Fig. 4b).

We calculated modal analysis up to the first 120 modes of vibration to summarize scores of total participating mass higher than the 85% in the X and Y directions and higher than 70% in the Z direction. Masses rates were significant

for the first few modes, and smaller but randomly distributed towards higher modes. The first two modal shapes were translational and symmetrical according to 45° axes, the third mode was torsional instead (Fig. 5). The following modes had mixed characteristics with localized excitations involving limited group of beams.

Assessment of the unloaded mock-up state (phase 2)

Numerous factors related to the assembly phase affected the shape of the mock-up. The structure was not free-standing until the end of such operation, and as an effect of tolerances, fabrication, and dry-assembly errors, the theoretical expected shape resulted altered. To consider this geometrical deviation, we introduced an inelastic representative vector field into the Voronoi perfect model.

Such field was known by calculating its shape and its relative amplitude. We built the shape of the vector field through a composition of modal eigenforms, given by the natural frequency analysis of GS_0 . In this phase, other fields were also considered, such as the deformed shape for uniform loading or for asymmetric loading and the main buckling eigenforms. We divided the whole surface into four homogeneous areas, identified by the X - and Y -oriented symmetry axes (Fig. 2a); then, we searched for the best eigenforms that locally approximated the unloaded (geometrically imperfect) mock-up. In this phase, the selection started from a visual analysis of the prototype and neglected local deformations.

For the amplitude of the vector field, we used the measurements obtained from a geometric survey with a laser level, evaluating the displacement in Z coordinate for an appropriate number of nodes. The modal shapes were scaled by an area factor calibrated on the real survey data. A quantitative criterion supported the choice of the best modal shape among the previously selected ones. Summarizing, the procedure adopted was the following:

- Such that $\delta_{z,r}$ is the vertical displacement measured by the geometric survey, and $\delta_{z,mode}$ is the one extracted from modal shape for the corresponding nodes; we run the ratios $\delta_{z,r}/\delta_{z,mode}$.
- The scale factor σ represented the average of all the previous ratios.
- By multiplying all components of the modal shape by the factor σ , we defined the entire vector field: $\delta_i = \sigma \delta_{i,mode}$, where $i = (x, y, z)$.
- We deducted the survey rate from the final value as $\delta_z = \sigma \delta_{z,mode}$ to estimate the error made at the control points; the square root of the sum of the squares value returned an indicator I of severity of the error.

By minimizing this indicator I , we selected and scaled the modal shapes 10, 12, and 13, for the areas identified, respectively, by apices N326, N312 and N333, N340 (Fig. 2a). In addition, boundary nodes of neighboring areas were scaled according to the two adjacent eigenforms, and the nodal coordinates obtained were mediated to avoid singularities and guarantee smoothness of the surface. The application of such displacement field to the GS_0 nodal coordinates returned the imperfect geometry. Finally, linear static analyses tested the acceptability of the imperfect model that manifested about the same stress field of GS_0 . The similarity between physical and numerical models is shown in Fig. 6.

Experimental static behavior (phase 3)

We studied the static behavior by means of tests performed under time-invariant load configurations, where the i th load

increment is maintained until the stabilization of the measure. The aim was to simulate the serviceability loading of the mock-up, transforming a distributed load into equivalent nodal forces. Due to the feasibility of the test, 16 nodes of the vault were loaded. Organized in groups of four, the 16 nodes were symmetrically located with respect to the axes of the prototype. Hollow metal discs, each weighing 125 g, constituted the applied load and were hanged to each node by means of a ligature and a double-hooked-end self-balancing steel element. Such metallic extremity had the advantage of reducing vibrations transmitted to the structure.

The four apices of the vault and then the two central nodes were instrumented with inductive displacement transducers HBM WA L 100, connected to an acquisition control unit HBM WPM 100. The arrangement is schematically represented in Fig. 7 a. All the experiments required an adaptable modular tubular substructure, which was intended for accommodating the equipment, not causing interference with the tests thus avoiding any data corruption. The same substructure was reused also in the dynamic tests phase to support the instruments. The executive process can be summarized in the following steps:

- Preparation, counting, and approaching of weights close to the nodes to be loaded.
- Transducers installation and check (in particular, verification of verticality because of the only Z -displacement monitoring); connection to control unit and verification of the correct operating of the measuring system.
- Test phase, in which at every load step, a weight per node was hanged (total of 16 plates, one for each hook).
- For each step, the load was maintained until the structure settled (Fig. 8).
- Control and verification of the continuous recording of the data.
- Photographic survey at the end of each stage.

Dynamic identification through OMA and impulsive tests (phase 4)

The parameters derived from the dynamic experimentation are natural frequencies, damping ratios, and modal shapes (Ewins 2000; Maia and Silva 1997). The high deformability of the prototype suggested the use of an output-only method, such as the operational modal analysis (OMA) (Zhang et al. 2005). In addition, we used impulsive excitation tests to give feedback to the OMA data. Fundamental assumptions for the dynamic tests are linearity, stationarity, and observability, and the test programming complied with these assumptions.



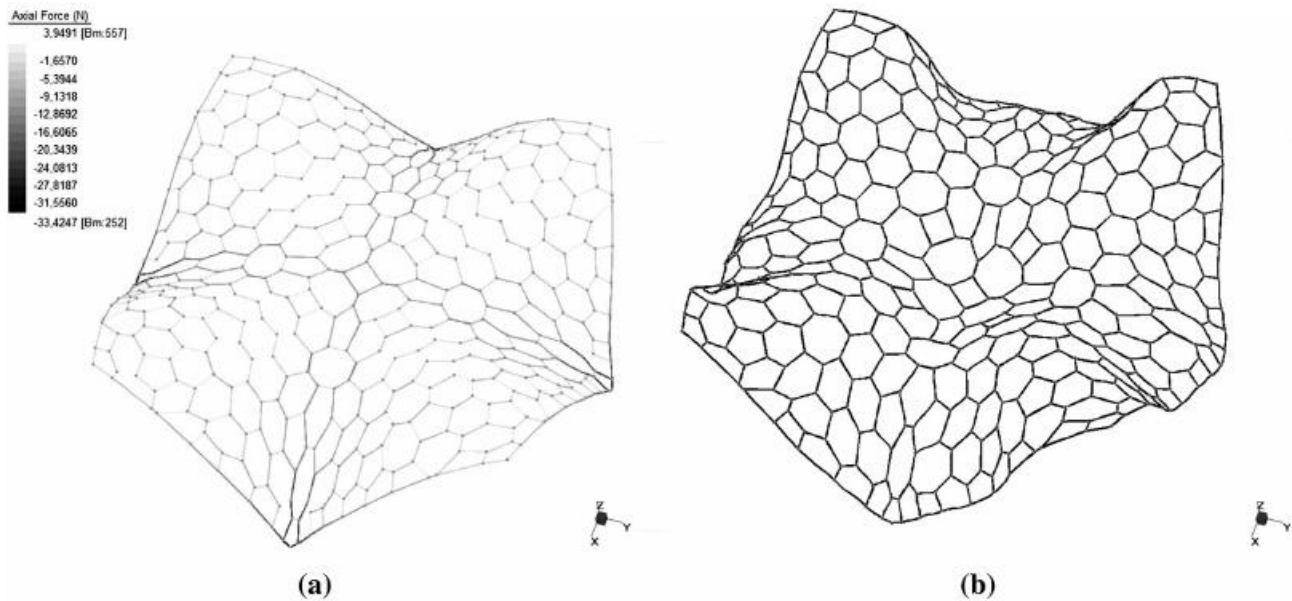


Fig. 4 GS_0 (perfect geometry model) linear static analysis under own weight: **a** beams axial forces (the darker the more axial compressed) and **b** global deformed shape

For vibration measurements, we employed capacitive accelerometers PCB Piezotronics Model 3701G3FA3G with magnetic mount, which exploited the presence of the metal washer on top of the nodes. All those transducers were connected to a multichannel acquisition unit LMS SCADAS III, endowed with the acquisition software LMS Test.Lab. Their orientation matched the local nodal coordinate system, and their positioning aimed at a uniform and symmetrical distribution on the surface also considering the defects highlighted from the previous analyses (Fig. 7b). For the hypothesis of observability, we considered the influence of the accelerometers mass in the subsequent numerical simulations. Accordingly, the position of these transducers was kept invariant during all the dynamic tests: indeed, the mass of ten accelerometers (100 g each) constituted a sensible loading for such a lightweight prototype, about 5% of the total vibrating mass. The signal noise was negligible, because the cables were lying on the tubular structure and lowering in correspondence of their relative transducer. The steps required by dynamic tests were the following:

- installation of the accelerometers, namely, checking, cleaning, numbering, positioning, and connection to cables;
- connection of the cables to the acquisition unit to verify the correct efficiency of the measuring system in free run;
- execution of the dynamic experimental test and data saving.

We performed three cycles of OMA tests, each for a sampling time of about 30 min. Two series of impulsive

dynamic tests followed. The first series consisted of 21 measurements with the impact hammer PCB Piezotronics Model 086D20, equipped with a transducer tip of average hardness 084A62 Tip—medium plastic (Fig. 8). The second series consisted in a sudden removal of a pre-stress condition from the mock-up. Practically, we constrained a gravitational mass, made of a group of metallic discs, to an FDM printed structural node by means of a link cable. Cutting such cable and letting the mass fall on a neoprene mat, the Voronoi vault resulted excited but unperturbed from the mass fall. The amount of measurements performed with this procedure was 4.

Results and modelling

Experimental static output and FEM static model

Figure 9 presents the main results of the static tests, performed as mentioned at paragraph 2.3. The numbering of the sensitive control nodes identifies the non-linear curves in the graph. We decided to exclude the first set from the results, because it was not deemed representative. Typically, measurements N326 and N333 had similar displacements in the Z-positive direction. The node N340 was less disposed to motion, and the node N312 had intermediate behavior and manifested a homothetic curve with respect to the displacements. The symmetric nodes N455 and N456 described very similar paths with significant increases in the gravity direction, about three times higher than those at the vertices. In addition, all the nodes

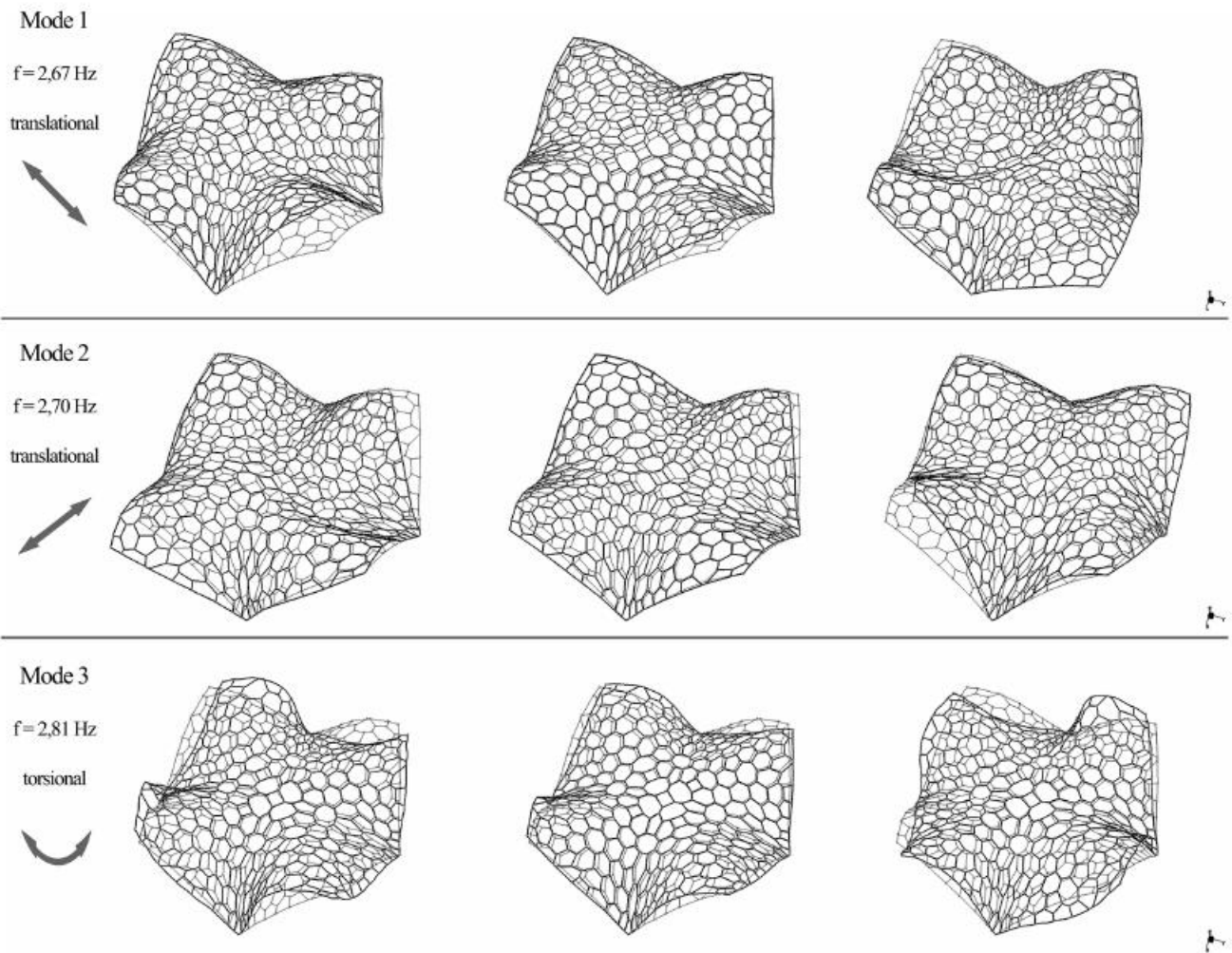


Fig. 5 Main modal shapes from GS_0 natural frequency analysis

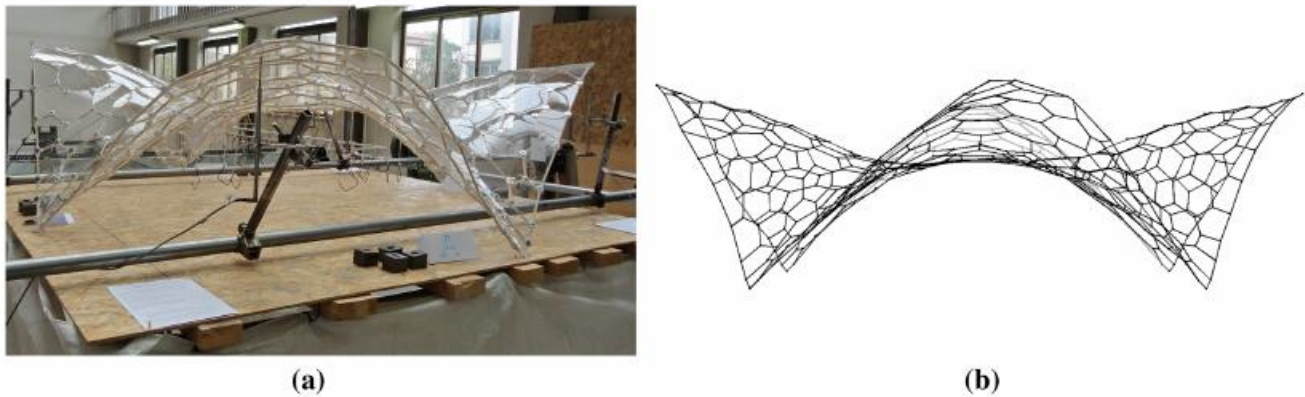


Fig. 6 Similarity between (a) the physical mock-up and (b) the representative FEM geometry built on the modal shapes of GS_0 and calibrated on the mock-up survey

displayed a significant irreversible deformation after the unloading, so the final curvature of the shell changed. Two main sources of non-linearities influenced the static response: high deformability of the prototype (namely

geometrical non-linearity) and the joints restraints. Indeed, because of the full contact in compression and the unpredictable friction in traction, the contact between the wooden beams and the nodes was non-linear. A similar but less

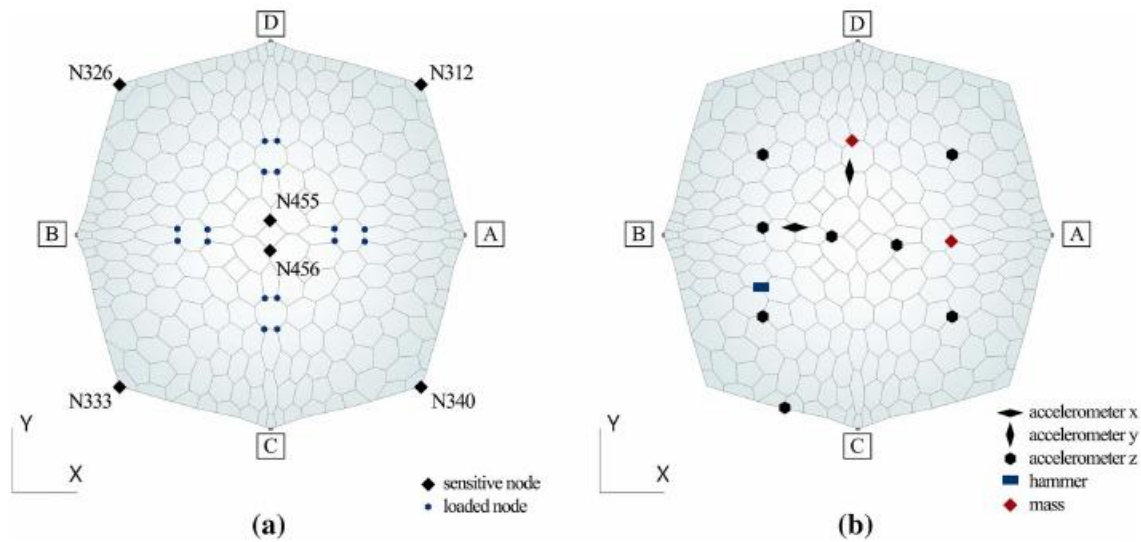


Fig. 7 Tests schemes and settings (top view of the vault): a static tests and b dynamic tests

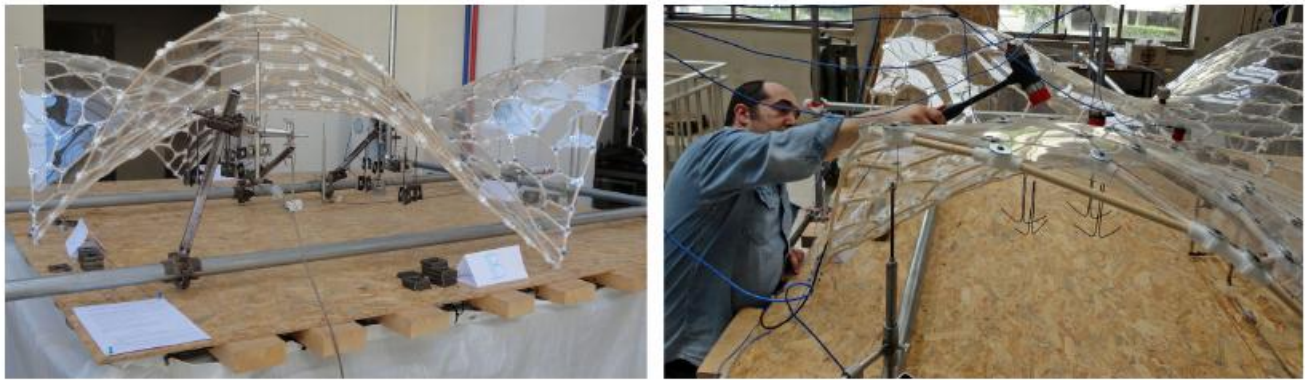


Fig. 8 Images from testing phases: on the left, the loading during static tests; on the right, the dynamic impulsive test with the impact hammer

important (in this loading condition due to the relative lower resistance) non-linearity was in the clamping system of the PET panel (full contact in compression, possible sliding in traction).

The calibrated FEM static model, named GS_1 , consisted of 465 nodes and 697 beam elements. Non-linear static analyses considering only geometric non-linearity were performed. As base geometry, we used the imperfect geometry from phase 2, and then, we scaled the mechanical characteristics such as the degree of constraint and the material properties to match the experimental behavior. The same 50 g nodal masses were loaded, since the PET panels were not modelled. We varied the beams properties to simulate both the non-rigid connection and the structural imperfections, fitting a global simplified modelling. Therefore, we approximated the Young's modulus with a secant average stiffness $E' = E/3$ over the limit of proportionality, and introduced elastic rotational releases of stiffness $k = 210,000$ Nmm. The rotational stiffness of the

springs was equivalent to that in conditions of semi-rigid connection for an average-length beam. The comparison between the experimental and numerical models (Fig. 10) proves the followed procedure. The introduction of elastic end releases is a simple and effective measure to introduce the effect of non-rigid connectivity in a global modelling (i.e., Hwang et al. 2009).

GS_1 linear analysis simulated only the conditions under own weight. As GS_0 analysis, it showed predominantly beams axial stresses and negligible bending moments. Due to the introduction of the unloaded deformed geometry, the displacement field became asymmetric.

Experiment dynamic output and FEM dynamic model

The algorithm Operational PolyMAX[®] processed the experimental dynamic OMA data. Figure 11 shows the auto-spectrum function concerning the frequency range

2–10 Hz for the third OMA test. The response peaks occurred essentially at the prototype natural frequencies of vibration. The results from the impulsive tests confirmed those obtained with the output-only tests (Fig. 12).

In general, all the OMA test lectures provided excellent agreement in terms of natural frequencies (Fig. 13 a). The first modes had a frequency range of 3–5 Hz, and the first three were, respectively, 3.45, 4.10, and 4.30 Hz. The damping ratio data were more variable (Fig. 13b), but limited in a maximum range of about 0.3%. In any case, damping ratios were never higher than about 1.7%.

The OMA Run 3 test was assumed as the most reliable and provided the parameters to study the modal shapes. Moreover, it returned one further mode of vibration (the 10th) that the other lectures did not. The representation of the OMA Run 3 eigenforms in the complex plane allowed calculating the mode degree of complexity. Drawing the least squares trend line for each modal shape, we observed that it was approximately horizontal and thus nearly parallel to the real axis. We asserted that the modes were ‘almost real’, which means that they were complex but with a meanly negligible imaginary component if compared to the real one. To confirm this achievement and to collect quantitative information, we applied the method MCF2 (Ewins 2000), whose indicator provides the percentage degree of mode complexity. The results for the first four modes of vibration (Fig. 14) highlight the low percentage of the MCF2 indicator according to the outcomes of the least squares trend line.

Consequently, it is possible to approximate the ‘almost real’ modal parameters as real, appraising the Voronoi vault as a classic civil structure, whose problem of dynamic equilibrium in the design phase is usually solved in not-damped vibrations condition. This consideration made also possible to compare test-observed data with an FEM model, in which the problem of dynamic equilibrium is also solved in not-damped free vibrations.

A new numerical model, named GS₂, was built on the phase 2 geometry to simulate the experimental dynamic behavior. As observed from the dynamic test, the experimental response resulted stiffer than the GS₀ natural frequency analysis (lacking of the modelling of panels). Because of the assumptions of linearity and small displacements, the nodes can be asserted as rigid, so with linear contacts, and the stiffness of secondary elements, such as the PET panels, as not negligible. The latter contributed indeed in the dynamic response as a bracing system for the Voronoi cell, so were modelled as ‘equivalent rods’. We installed a sheaf of one-dimensional elements between the centroid and the vertices of the Voronoi polygon of each cell. Centroids were moved in deformed configuration following the procedure in previous 2.2. Not knowing the stiffness of the PET panel, the evaluation of the equivalent rod section followed a criterion of average area equivalence. Rod elements had 40 × 1 mm section, null density (because the panel dead load was already present as a nodal mass) and Young’s modulus $E_p' = E_p/3$. Figure 15 presents the GS₂ FEM global model and one of its cell. The model consisted of 696 nodes and 2009 beam elements.

A comparison with the numerical model was possible only in terms of natural frequencies and modal shapes. The concordance between the models can be appreciated in Fig. 16, in particular for the first nine modes, while the gap becomes noticeable at increasing but less important frequencies.

The comparison between the FEM GS₂ modal shapes and the test-observed data is possible only if the experimental eigenforms are converted into ‘real’ vectorial fields. Since the modal shape is defined up to a constant, it is allowed to project the complex experimental amplitudes of modal coordinates on the least squares trend line (dashed line in Fig. 14).

For the first four modes of vibration, the experimental and numerical amplitudes are compared in the first column

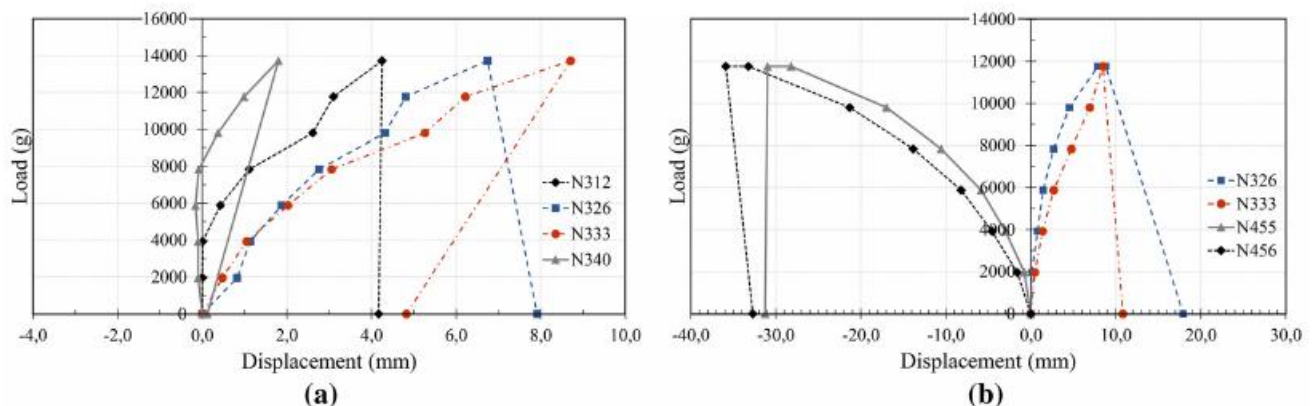


Fig. 9 Results of the static tests: **a** Z-displacement monitoring of the four top nodes of the vault (test n. 2) and **b** Z-displacement monitoring of two top nodes and two center nodes of the vault (test n. 3)

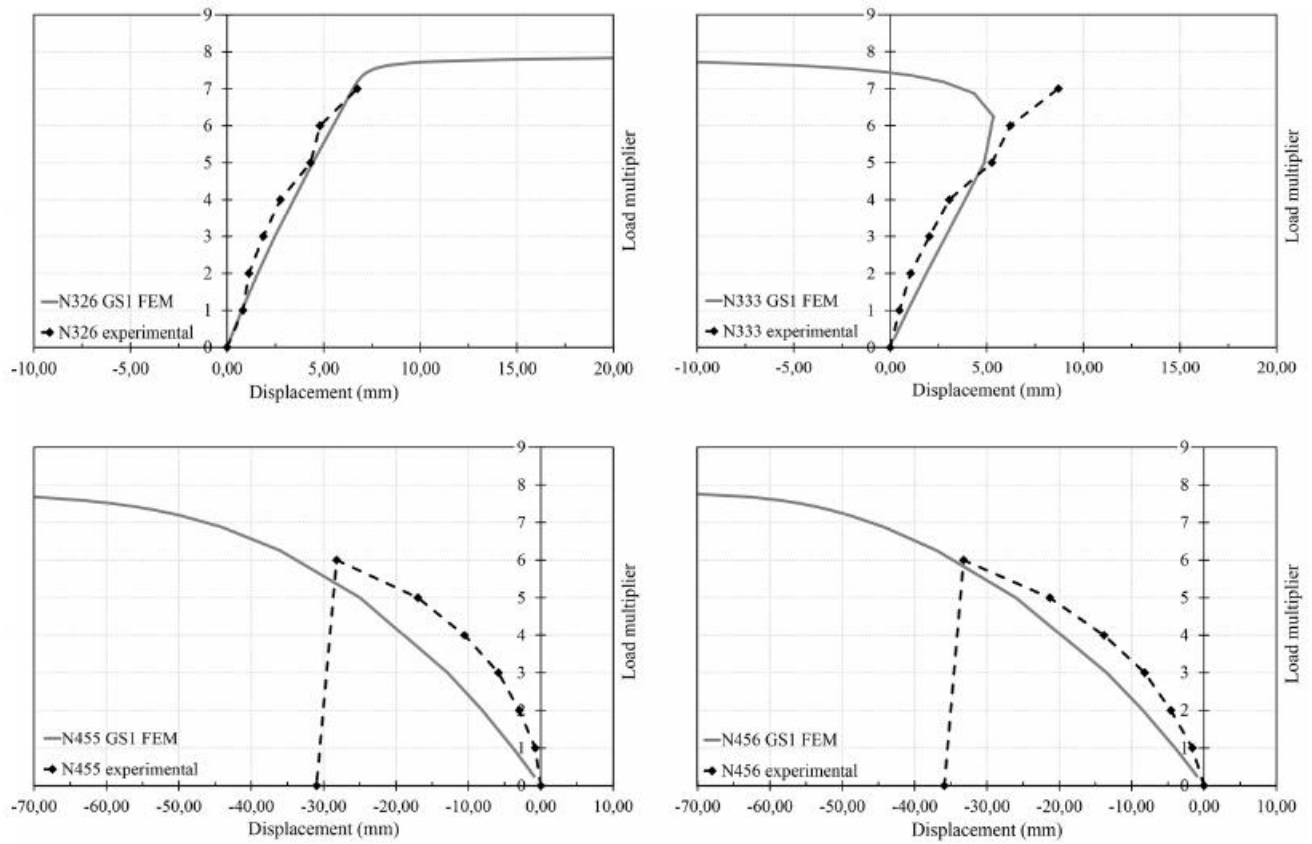
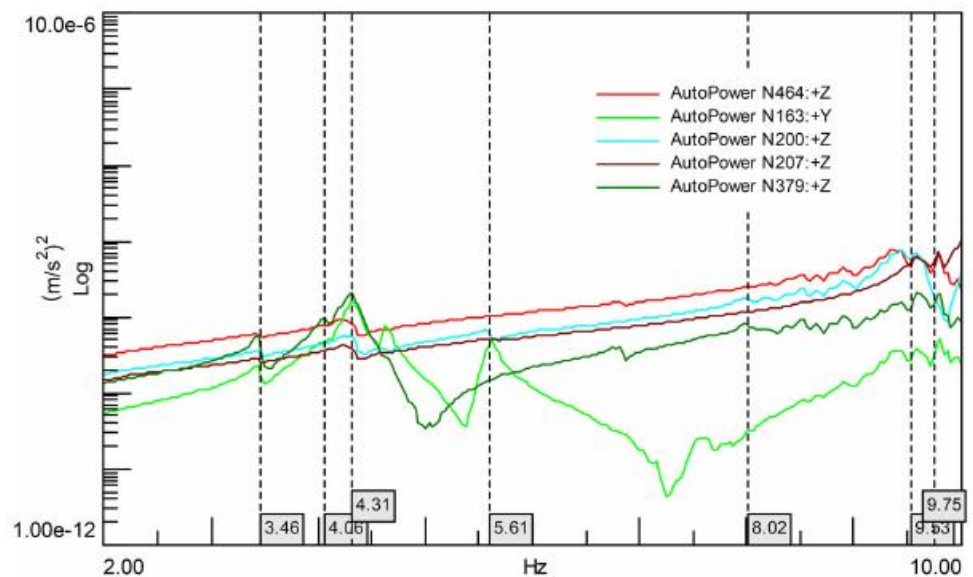


Fig. 10 Comparison in terms of displacement between GS_1 (continuous line) and experimental static tests output (dashed line): on the first row, top nodes of the vault; on the second row, center nodes of the vault

Fig. 11 OMA Run 3 test: power spectral density function with highlighted the modal frequencies



of Fig. 17. The closer the two data set points in the ordinate direction, the more representative is the GS_2 model for that experimental degree of freedom (DOF) amplitude. Note that the polyline has no analytical meaning, because the DOFs examined were not in that relative spatial relation.

The middle column of Fig. 17 reports the modal experimental shape as vectors at each monitored DOF (red positive local z coordinate, blue negative) to be compared with the last column, in which are the GS_2 eigenforms, obtained from numerical natural frequency analysis.

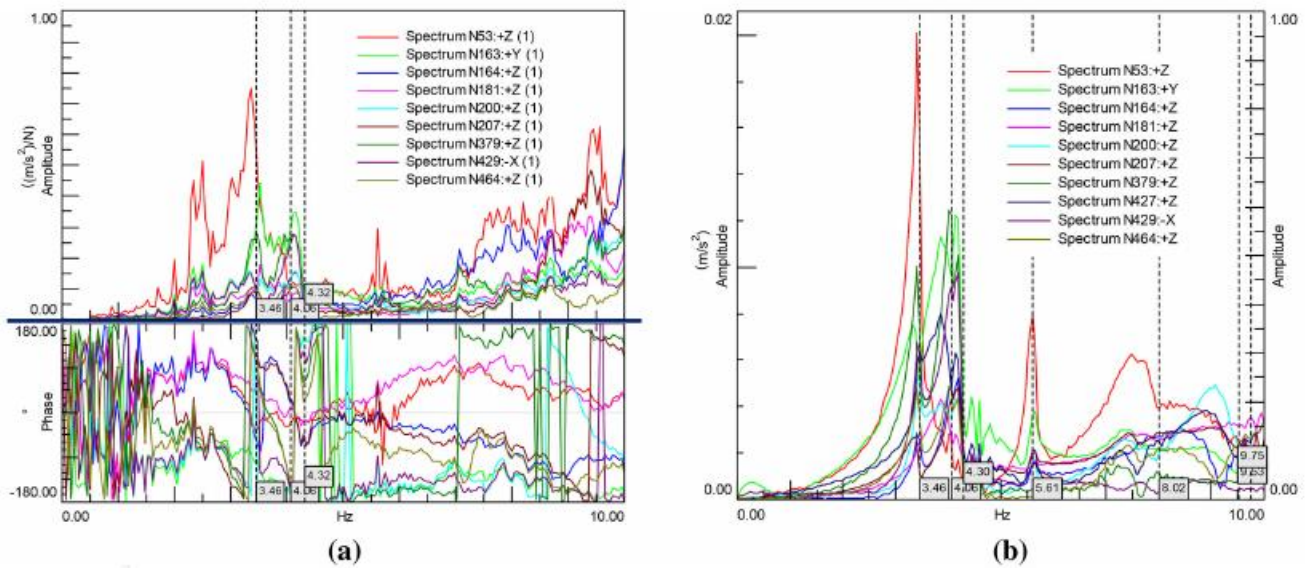


Fig. 12 Frequency Response Function (FRF) with highlighted the modal frequencies: **a** N416 hammer (test n. 17) and **b** N263 mass (test n. 4)

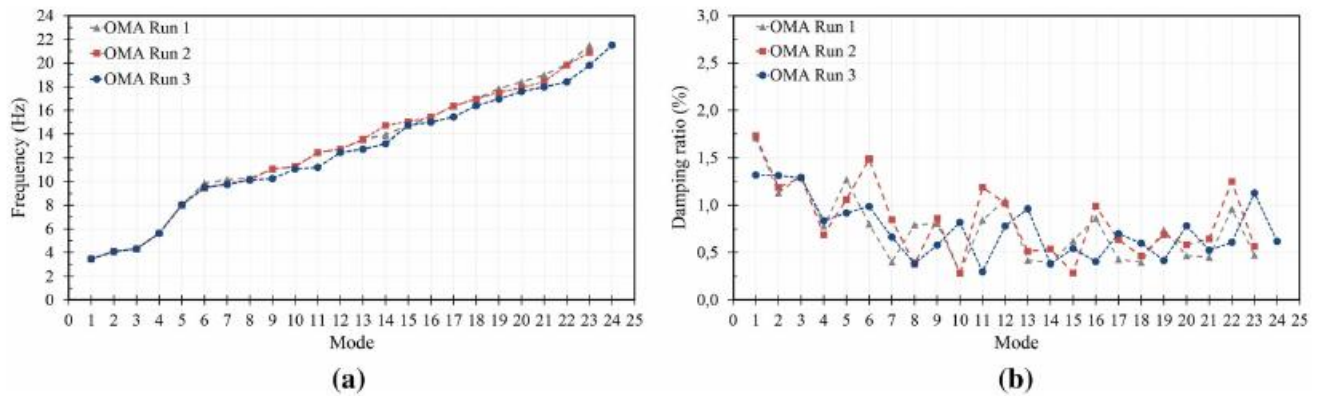


Fig. 13 Comparison between OMA readings: **a** natural frequencies and **b** damping ratios

Finally, the GS_2 modal analysis showed the prevalence of the first three modes in relation with the higher participating masses (about 50% of the total vibrating mass in X and Y directions for the first three modes) and the presence of a global motion. The upper ones achieved small increments of vibrating mass, totalizing about 85% in X and Y directions and about the 75% in Z direction while considering the first 90 modes. Both the FEM and the prototype had a torsional first mode, the next two (second and third) mainly translational but also with little torsional components, and the fourth torsional again. Higher modes have local characters.

Discussion

The method used within this work concerns the Voronoi static-aware vault, but is extendable to other Voronoi static-aware case studies. Simulating the size and the state of

the mock-up, a disadvantage is that the findings are strictly related to the specific shape, internal tessellation, building technology, materials, and local errors of assembly.

The stiffness of the joints, the structural imperfections, and the non-linear behavior of the connections played the most significant role in the present research. Indeed, modelling assumptions of joints and material properties in the GS_0 perfect geometry were not representative of the physical evidence. Internal connections were in practice not rigid and the nodes showed significant anomalies: they reacted when receiving the beams in compression, while offered only scattered and unpredictable frictional resistance in response to tension forces. This non-linearity would require a lot of efforts and expertise for the calibration of detailed local models or an adequate probabilistic model. Because the aim of this work is to produce simplified global FEMs, such extensive research is referred to further work. Considering the simplifications adopted in

the construction of the phase 2 geometry, particularly the neglecting the localized deformation of the prototype and the use of a unique mean value of rotational stiffness for all the beams, the matching of the FEM static model with the experienced data can be viewed as acceptable.

As an assumption to this work, we considered only symmetrical loading cases. Two reasons did not allow to consider asymmetrical loading: first, the geometric imperfection at the unloaded state and second, the high deformability of the mock-up. The deviation of the initial

geometry from the theoretical model influenced the structural behavior, producing asymmetrical displacement fields and asymmetrical modal shapes although the symmetrical loading. Hence, asymmetrical loading would have complicated the structural identification of the mock-up. Moreover, since the lowest collapse multiplier is usually associated with asymmetrically loaded grid shells, the Voronoi vault would have prematurely drawn its ultimate limit state for the same (or even lower) loading rates, being the vault not optimized for asymmetric loading conditions.

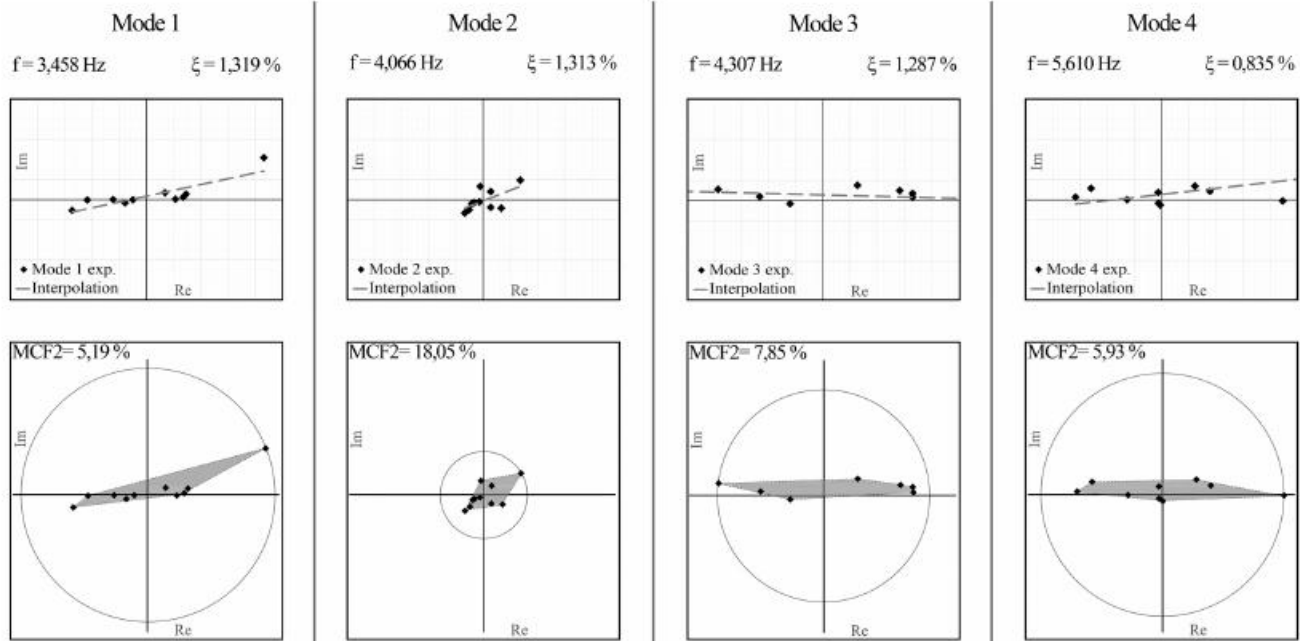


Fig. 14 Evaluation of complexity of the experimental modal shapes: on the *first row*, representation of the modal shapes with the interpolating line; on the *second*, MCF2 method

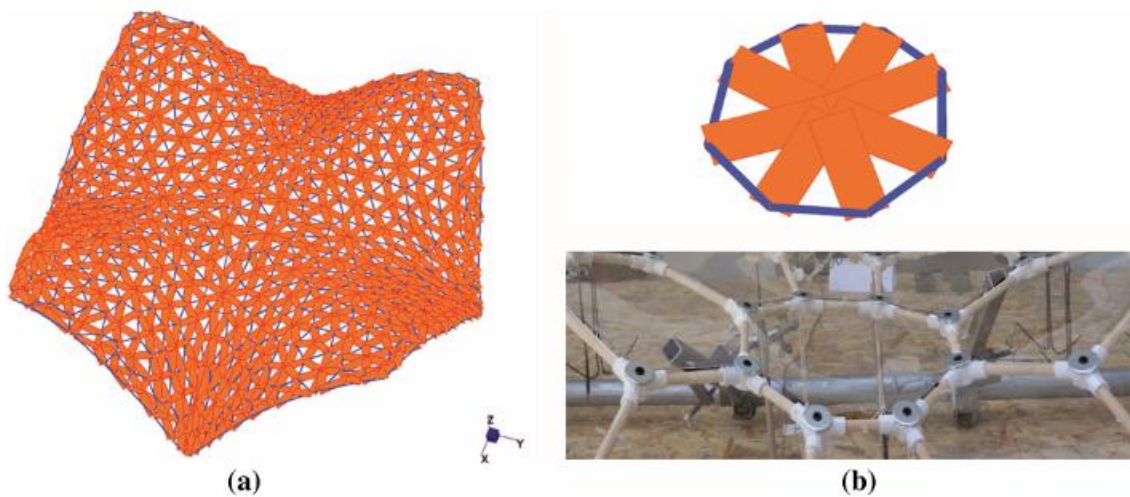
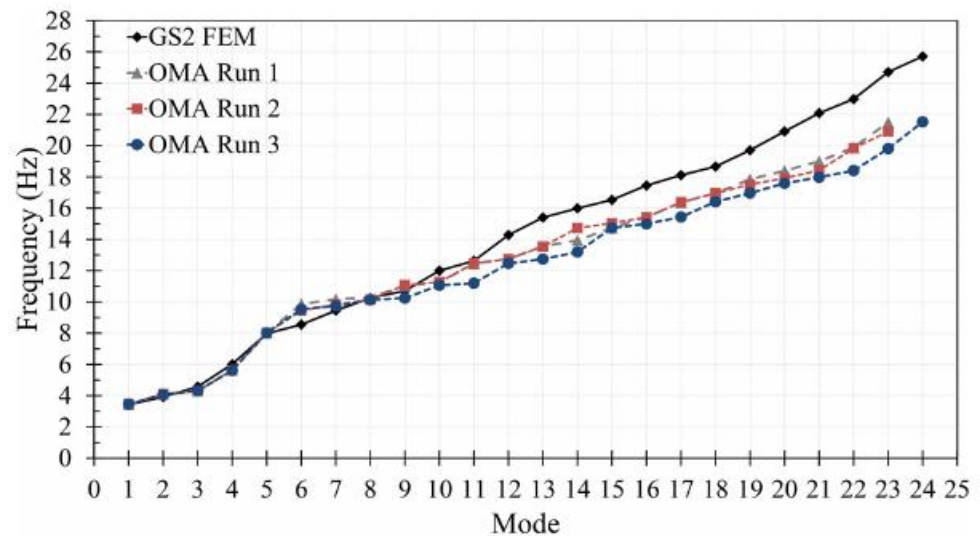


Fig. 15 GS₂: **a** finite-element model and **b** generic Voronoi cell panel modelled as equivalent rods

Fig. 16 Comparison between GS_2 and OMA tests output: modal frequencies



A complete validation for the Voronoi tessellation in the presence of asymmetric loading is demanded to future works, as well as investigations on the effect of additional stiffening contribution given by bracing cables.

The assessment of the prototype state before the tests resulted in a base geometry used in the following GS_1 and GS_2 FEM models. The vector field denoted only geometrical imperfection of that specific mock-up. Shape similar structures and scaled structures could not manifest the same deformation. Unfortunately, there is no evident rule on the selection of the vector field components. The only criterion was the best fitting of the imperfect real structure. The selected modal shapes of GS_0 indeed are not even the most significant in the dynamic behavior.

The experimental tests required a considerable initial effort, regarding their conception, and attentions at runtime to minimize the chance of interference with such a high deformable prototype. Although the resolution of the tests was quite low, indications obtained were sufficient for the calibration of simplified FEM simulations. Concerning the modelling experience, we developed two separate FEM models for the static and dynamic behaviors, both different from the perfect one. The characteristics of the main representative FEM models are summarized in Table 1. The models were created to match the experimental behavior, and their potential use for a buckling analysis needs careful attention because of the arduous task to select the correct equivalent geometrical imperfection (suitable sizes and shapes, as per CEN 2009; Bacco and Borri 1993; Bulenda and Knippers 2001; Schlaich and Schober 1997) in such a simplified model.

The reproducibility of the static tests is linked essentially to non-linearity problems and to their random

distribution. Similar scheduled tests have shown similar trends but different amplitudes of displacement and inelastic behavior at the unloading. Finally, we also observed some small cracks at the nodes and little but important localized sliding of the beams from their nodal plastic casing. The mock-up non-linearities and the complicated internal mechanisms of load dissipation are topics on which focusing for future works and for improving the prototypes design. On the other hand, the dynamic tests are reproducible because of their minute loading and the linearity of the mock-up.

The dynamic behavior expected from the prototype was a combination of complex motions, typical of an irregular structure, characterized by local excitations. The GS_0 model manifested as the unique exceptions the first two translational and symmetric modes. The real dynamics of the mock-up showed considerable differences due to the loss of symmetry for the superimposition of the initial geometrical deviation. The first eigenform was torsional indeed. The general growth of the torsional components implies the impossibility to simplify the behavior of the structure and indicates a not-uniform distribution of stiffness and in all likelihood of damping too.

In the dynamic tests, the number of accelerometers was enough to determine frequencies and damping ratios but not to acquire high-resolution modal shapes. A better test would have used miniaturized transducers, overlapping the acquisitions of different measurements. Such procedure would have complied with the observability hypothesis because of the neglecting of the instruments mass. Despite our assets, we concluded that it is possible to make a simpler dynamic analysis, considering our case study as a not damped system. This result appears to be one of the most relevant and pragmatic findings.



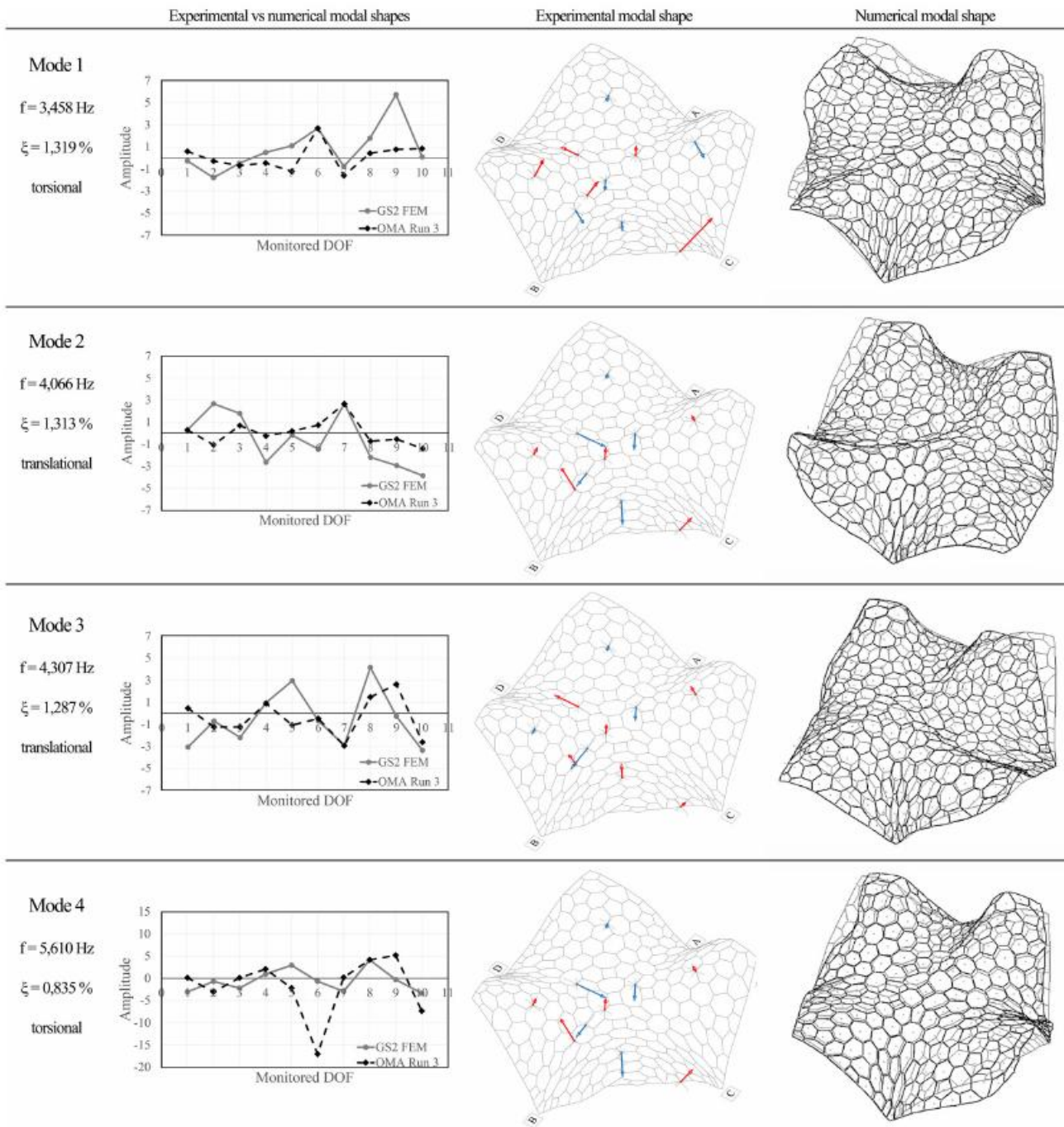


Fig. 17 Comparison between GS₂ and OMA test output for the first four modal shapes

Conclusions

This paper examined a static-aware Voronoi free-form grid shell vault through experimental tests. Numerical simulations followed. The obtained results can be used as first step to gain a better understanding of the behavior of such novel hex-dominant grid shells.

In perfect geometry modelling, the generated stress field and the distribution of compression stresses confirmed the work of the static-aware Voronoi algorithm in providing promising design alternative to build grid shells. Nonetheless, some assumptions of this form-generation phase were removed to describe the statics and dynamics highlighted during tests performed at the

Table 1 Modelling parameters of the FEM models

	Base geometry	E (N/mm ²)	E_p (N/mm ²)	k_{beams} (Nmm)	$k_{\text{eq,PETrods}}$ (Nmm)
Characteristic values	–	11,000	3700	–	–
GS ₀	Perfect	11,000	0	∞	–
GS ₁	Imperfect as per phase 2	3700	0	210,000	–
GS ₂	Imperfect as per phase 2	11,000	1200	∞	0

Structural Laboratory of University of Pisa. Two FEM models were calibrated on the test-observed data. FEM analyses were conducted on a base geometry acquired from scaling the modal eigenforms with respect to a geometrical survey.

The basic findings from the static test phase and modelling were as follows:

- Clearly non-linear experimental behavior since the earliest loading phases (geometrical non-linearity).
- Experimental output influenced by initial shape, local non-linearities and stiffness of the joints.
- A static FEM model setting a beams secant elastic modulus ($E/3$) and semi-rigid internal nodes drew with an adequate approximation the experimental behavior. The panels are considered in the model as a dead load only.

From the dynamic test phase and analysis, the following findings were observed:

- Excellent agreement between OMA and impulsive tests.
- ‘Almost real’ test-observed modes of vibration, the advantage was that we could neglect the influence of damping in the problem of dynamic equilibrium and warrant comparison with numerical modes obtained in non-damped free vibrations.
- A dynamic FEM model considering the PET panel influence in the dynamic response, modelled as star-shaped equivalent rods, matched the experimental frequencies and modal shapes.

Acknowledgements The authors would like to acknowledge Dr. Ing. Davide Tonelli for his valuable collaboration, Prof. Ing. Paolo S. Valvo, Dr. Ing. Giuseppe Chellini and Mr. Michele Di Ruscio for the competent support provided during the experimental tests.

Open Access This article is distributed under the terms of the Creative Commons Attribution 4.0 International License (<http://creativecommons.org/licenses/by/4.0/>), which permits unrestricted use, distribution, and reproduction in any medium, provided you give appropriate credit to the original author(s) and the source, provide a link to the Creative Commons license, and indicate if changes were made.

References

- Adriaenssens S, Ney L, Bodarwe E, Williams C (2012) Finding the form of an irregular meshed steel and glass shell based on construction constraints. *J Archit Eng* 18(3):206–213
- Adriaenssens S, Block P, Veenendaal D, Williams C (2014) Shell structures for architecture: form finding and optimization. Routledge, New York
- Bacco O, Borri C (1993) Post-buckling behaviour of perfect and randomly imperfect grid shell structures. In: *Space Structures 4: Proceedings of the fourth international conference on space structures*, pp 1–9
- Baldassini N et al (2010) New strategies and developments in transparent free-form design: from faceted to nearly smooth envelopes. *Int J Sp Struct* 25(3):185–197
- Bulenda T, Knippers J (2001) Stability of grid shells. *Comput Struct* 79(12):1161–1174
- Cai J, Gu L, Xu Y, Feng Y (2013) Nonlinear stability analysis of hybrid grid shells. *Int J Struct Stab Dyn*. doi:10.1142/S0219455413500065
- CEN European Committee for Standardisation (2009) Eurocode 3: design of steel 327 structures-Part 1-1: general rules and rules for buildings. EN 1993-1-1, Brussels (Belgium) 2005 (last revision March 2009)
- Dini M, Estrada G, Froli M, Baldassini N (2013) Form-finding and buckling optimization of grid shells using genetic algorithms. In: Obrebski JB, Tarczewski R (eds) *Beyond the limits of man*. IASS, Wroclaw, pp 210–215
- Ewins DJ (2000) *Modal testing: theory, practice and application*, 2nd edn. Research Studies Press Ltd, Baldock
- Gioncu V (1995) Buckling of reticulated shells: state-of-the-art. *Int J Space Struct* 10(1):1–46
- Hwang KJ, Knippers J, Park S-W (2009) Influence of various types of node connectors on the buckling loads of grid shells. In: *Symposium of the International Association for Shell and Spatial Structures (50th. 2009. Valencia)*. Evolution and Trends in Design, Analysis and Construction of Shell and Spatial Structures: Proceedings. Editorial Universitat Politècnica de València
- Jiang C, Wang J, Wallner J, Pottmann H (2014) Freeform honeycomb structures. *Comput Gr Forum* 33(5):185–194
- Jiang C, Tang C, Vaxman A, Wonka P, Pottmann H (2015) Polyhedral patterns. *ACM TOG* 34(6):172
- Maia MMM, Silva JMM (1997) *Theoretical and experimental modal analysis*. Research Studies Press LTD, Baldock
- Pietroni N, Tonelli D, Puppo E, Froli M, Scopigno R, Cignoni P (2015) Statics aware grid shells. *Comput Gr Forum (Special issue of EUROGRAPHICS 2015)* 34(2):627–641
- Pottman H (2009) Geometry and new and future spatial patterns. *Archit Des* 79(6):60–65
- Pottmann H (2013) Architectural geometry and fabrication-aware design. *Nexus Netw J* 15(2):195



- Pottmann H et al (2007) Geometry of multi-layer freeform structures for architecture. *ACM TOG* 26(3):65
- Sassone M, Pugnale A (2010) On the optimal design of glass grid shells with planar quadrilateral elements. *Int J Sp Struct* 25(2):93–105
- Schlaich J, Schober H (1996) Glass-covered grid-shells. *Struct Eng Int* 6(2):88–90
- Schlaich J, Schober H (1997) Glass roof for the hippo house at the Berlin Zoo. *Struct Eng Int* 7(4):252–254
- Tonelli D (2015) Statics aware voronoi grid-shells. PhD Dissertation, University of Pisa
- Tonelli D, Pietroni N, Puppo E, Froli M, Cignoni P, Amendola G, Scopigno R (2016a) Stability of statics aware Voronoi grid-shells. *Eng Struct* 116:70–82
- Tonelli D, Pietroni N, Cignoni P, Scopigno R (2016b) Design and fabrication of grid-shells mockups. In: *STAG: Smart Tools and Apps for Graphics*, Eurographics Association 2016
- Zhang L, Brincker R, Andersen P (2005) An overview of operational modal analysis: major development and issues. In: Brincker R, Møller N (eds) *Proceeding of 1st international operational modal analysis conference*. Aalborg Universitet, Copenhagen, pp 179–190